Journal of Applied Fluid Mechanics, Vol. 18, No. 3, pp. 728-741, 2025.
Available online at www.jafmonline.net, ISSN 1735-3572, EISSN 1735-3645.
https://doi.org/10.47176/jafm.18.3.2906

Modelling and Optimization of Fluid Frictional Torque in a Single Stage Centrifugal Pump with a Vaned Diffuser Based on RSM, ANN and Desirability Function

K. Singh†, A. Singh and D. K. Singh

Department of Mechanical Engineering, NSUT, New Delhi 100078, India

†*Corresponding Author Email: kamal.phd21@nsut.ac.in*

ABSTRACT

In a centrifugal pump, the clearance flow is quite common due to the existence of clearance between the casing and impeller. Apart from the clearance, the impeller speed and flow rate have a significant impact on fluid frictional torque. This study uses experimental and numerical methods to investigate these dynamics. The experimental setup includes measurements of fluid frictional torque at various levels of axial clearance (0.6 mm, 1.2 mm, and 1.8 mm), flow rates (8 L/min, 10 L/min, and 12 L/min), and impeller speeds (800 rpm, 1000 rpm, and 1200 rpm). A 3-level, 3-factor factorial design (L_{27}) is employed to systematically examine the impact of these factors on fluid frictional torque. Response Surface Methodology (RSM) and Artificial Neural Networks (ANNs) are utilized to capture complex parameter interactions, with optimization performed using a Desirability Function (DF). The analysis reveals a significant increase in fluid frictional torque with increasing axial clearance, impeller speed, and flow rate. The optimal operational parameters for minimizing fluid frictional torque in the centrifugal pump are identified as $\omega = 888.94rpm$, $Q = 8.026L/min$ and $C_f = 0.619$mm, achieving a minimum fluid frictional torque of 0.499 Nm

Article History:

Received June 14, 2024
Revised September 24, 2024
Accepted October 18, 2024
Available online January 1, 2025

Keywords:

Fluid frictional torque
ANOVA
RSM
ANN
Optimization

1. INTRODUCTION

Centrifugal pumps play a vital role in engineering applications, constituting a significant portion of the world's total energy consumptions. Designers continuously strive to enhance the efficiency of these pumps due to their significant importance across diverse industries, including marine propulsion, water diversion, and agricultural irrigation (Zhang et al., 2015; Qiu et al., 2018; Zhao et al., 2020, 2022). The fluid frictional losses and disk friction losses, which are major losses in centrifugal pumps are closely linked to clearance flows between the impeller shrouds and casing covers. This relationship is particularly notable in pumps featuring open or semi-open impellers. Moreover, clearance flows not only affect the primary flows directly but also lead to indirect hydraulic losses to some degree by disrupting the main flow (Gülich, 2003). Engineering designs often overlook the intricate clearance flow to cut expenses. Research on flow dynamics in centrifugal pumps has predominantly concentrated on impeller and volute flow patterns (Kaupert & Staubli, 1999; Pedersen et al., 2003; González & Santolaria, 2006; Liu et al., 2013; Stel et al., 2013; Gao et al., 2014). Consequently, side chambers are frequently disregarded in computational forecasts of flow dynamics within centrifugal pumps equipped with shrouded impellers. Instead, empirical equations are employed to approximate centrifugal pump losses. Nonetheless, in numerous shrouded centrifugal pumps, clearance flows exert significant influence on pump efficiency and flow stability (Pei et al., 2012). Historically, engineers heavily relied on their expertise for the design optimization of centrifugal pumps, particularly due to large number of design parameters (Xie et al., 2018; Zhang et al., 2020; Song et al., 2024; Yang et al., 2022a). For example, Ma et al. (2018) presents a comprehensive investigation into optimizing the shape of a ring cavity to enhance the operational stability of a centrifugal compressor. Through rigorous analysis and comparison of optimization algorithms, particle swarm optimization emerges as the most effective approach for achieving global optimal solutions. The conventional optimization methods typically entail an iterative loop, wherein geometry parameters change manually to obtain the desired pump performance. This process involves

NOMENCLATURE

C_f	axial clearance	Cont. %	Contribution ratio
P_f	power corresponding to fluid frictional torque	**Abbreviation**	
P_m	power corresponding to mechanical torque	DF	Desirability Function
R^2	determination coefficient	DOF	Degree of Freedom
T_f	fluid frictional torque	MS	Mean Square
T_m	mechanical torque	ANN	Artificial Neural Network
T_o	total torque	RSM	Response Surface Methodology
Q	volumetric flow rate	SM	Sum of Square
ω	impeller speed	ANOVA	Analysis of Variance

numerical and experimental tests until the specified requirements are met (Zhu et al., 2018). Due to geometry complexity and large number of parameters involve in centrifugal pump, it is challenging to address them all simultaneously (Song et al., 2021; Xiang et al., 2022; Yang et al., 2022b). As a result, optimizing pumps with their complex design constraints solely through trial-and-error methods has become a challenging task. Orthogonal testing involves identifying critical factors to minimize trial iterations, but the computational costs increase during the optimization process (Kergourlay et al., 2007; Yuan et al., 2017; Ekradi & Madadi, 2020). As computational technology evolves, optimization problems benefit from numerous numerical techniques. One notable method is the machine learning algorithms which is based on a cycle of data collection, preprocessing, model training, evaluation, deployment, and iteration, enabling computers to learn from data and make intelligent decisions or predictions in various domains Alzubi et al. (2018)**.** In response to contemporary challenges, ANNs models have arisen as replacements for CFD analysis (Wang & Shan 2006; Derakhshan et al., 2008; Zhao et al., 2015; Ghadimi et al., 2019; Pei et al., 2019; Han et al., 2020; Massoudi et al., 2022; Gan et al., 2023). In their study, Wang et al. (2019) utilized an ANNs model to optimize a centrifugal pump combine with Design of Experiments (DoE), this network facilitated a computationally accessible solution. However, their optimization endeavours underscored the need for an accurately predictive ANNs model, which could result in an excess of points in less promising regions. To advance ANNs-optimization, sophisticated algorithms are required that can approach the global optimum point and converge more rapidly. As an example, Owoyele et al., (2021a) introduce an active learning-based optimization method efficiently explores complex design spaces, employing both exploration and exploitation strategies to reduce function evaluations compared to traditional methods. Applied to multi-modal surface and internal combustion engine design, it showcased significant promise, lowering the number of evaluations needed by up to 80%. These results highlight its potential for enhancing engineering optimization processes, with further refinement promising even greater efficacy in practical scenarios. This is achieved by removing the dependency on Design of Experiments (DoE) for training the ANNs models and implemented ActivO as a promising tool for engineers and researchers seeking to optimize designs in diverse fields, offering a pathway towards more efficient, sustainable, and innovative solutions. This approach has demonstrated exceptional effectiveness in pinpointing the global optimum Owoyele et al., (2021b).

In this research, we present a novel and comprehensive approach to the design of efficient centrifugal pumps, focusing on the crucial factor of fluid frictional torque in turbulent flow within pumps equipped with vaned diffusers. While the literature provides abundant information about the effect of clearance on calculating pump characteristics, there is a noticeable gap in research considering flow rate and impeller speed. To address this, we conducted both factorial and unifactorial designs to see the effect of axial clearance along with impeller speed and flow rate. To further enhance the depth of analysis, response surface methodology (RSM) and artificial neural networks (ANNs) employed. Subsequently, utilized optimization approach, by employing the desirability function (DF). This methodology allowed us to determine the minimum fluid frictional torque at optimal parameters such as speed (ω), axial clearance (C_f), and flow rate (Q). The innovative use of RSM, ANN and the optimization approach using the DF provide a nuanced and practical perspective for designing pumps.

2. EXPERIMENTAL PROCEDURE

2.1 Experimental Setup

The single-stage, low specific speed (N_s = 37) centrifugal pump with diffuser vane was tested at the fluid mechanics laboratory at NSUT, New Delhi, India. The geometrical details of the centrifugal pump are shown in Table 1, while the experimental procedure is outlined in the flow diagram in Fig. 1.

In this study the axial clearance can change by installing three sleeves with thickness of 0.6mm each, denoted as C_f.The impeller could move axially within the pump casing. In addition to the Pump Casing and its electrical motor the setup was equipped with a pressure transducer, a tank for water supply and storage, a flow meter, an energy meter for measuring voltage, current, energy consumption and power factor, a gated valve for controlling the flow of delivery side, a variant transformer to control the speed of electrical motor, a laser-based tachometer for measuring speed of impeller. The D52-2066 multi-function meter facilitates the simultaneous measurement of six parameters with a precision of 1%. These parameters comprise current (ranging from 0 to 100A), voltage (from 40 to 300V), power (0 to 30,000W), frequency (45 to 65Hz), energy consumption (0 to 99,999 kWh), and power factor (ranging between 0 and 1). A laser-based non-contact tachometer is utilized to gauge the

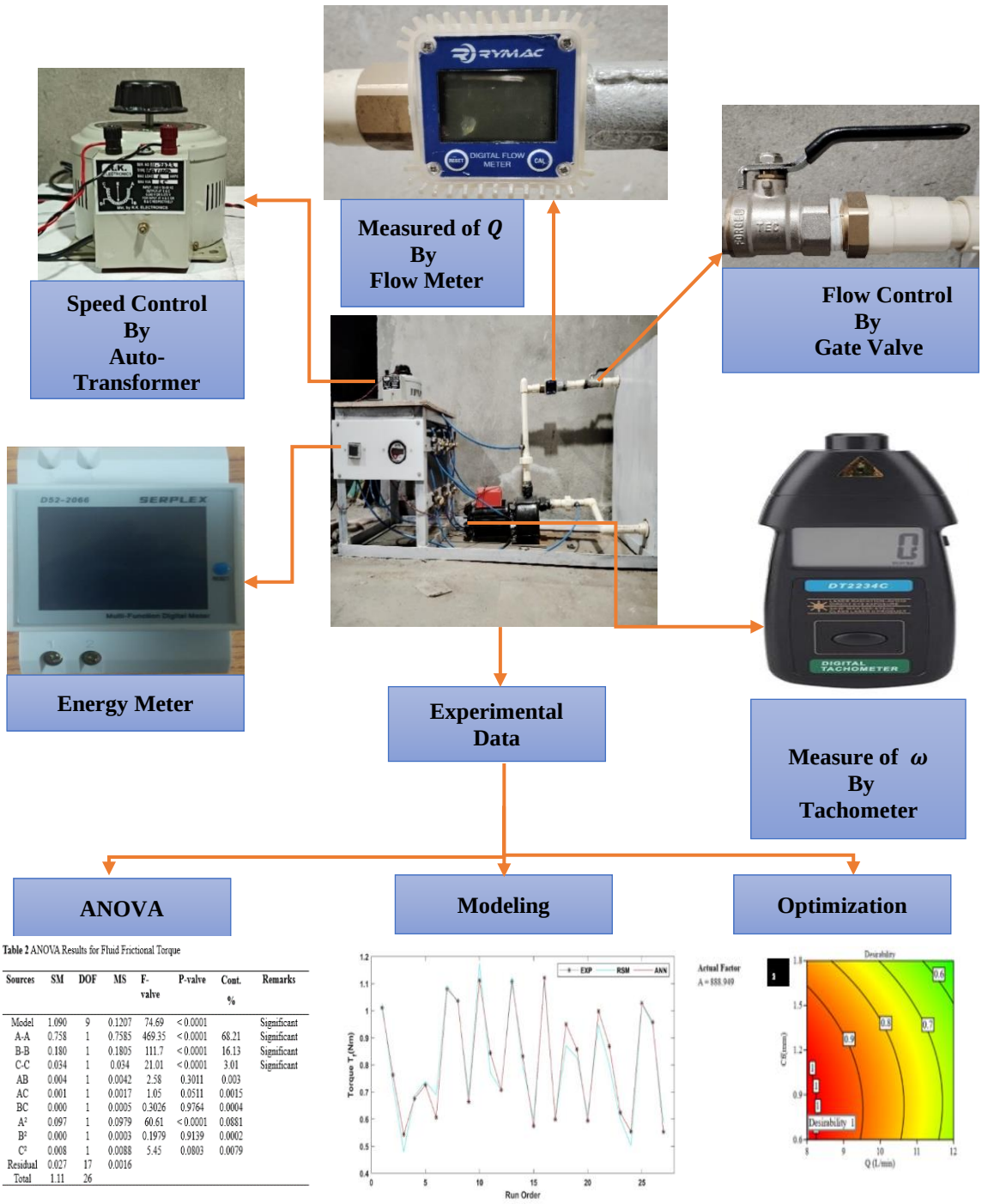

Fig. 1 Flow diagram of the experimental procedure

Table 1 Geometrical details of the centrifugal pump

Impeller inlet diameter, D_1	47mm
Impeller outlet diameter, D_2	127mm
Number of blades on impeller, Z_1	5
Impeller outer angle, β_1	30^0
Inner diameter of diffuser, D_3	130mm
Outer diameter of diffuser, D_4	180mm
Inlet angle of diffuser, β_2	16^0
Number of blades on diffuser, Z_2	5

speed of impeller, offering a range of 2.5 to 99,999 rpm with an accuracy of ±0.05%. Additionally, a digital flow meter is employed for measuring flow rates within the range of 5 to 120 L/min, boasting an accuracy of ±1%. To regulate the speed of the electrical motor driving the centrifugal pump, a variable transformer can adjust the voltage within the range of 0 to 270V. The estimated measuring uncertainties for fluid frictional torque is 1.41%. The objective of the experiment is to know the effect of axial clearance, flow rate and speed of impeller on fluid frictional torque. In the investigation of fluid frictional torque within centrifugal pumps, the total torque T_o, can be delineated into two constituent parts, as expressed by Eq. (3a).

$$T_o = T_m + T_f \quad (3a)$$

This equation highlights that the total torque T_o, is the summation of the mechanical torque (T_m) and the fluid frictional torque (T_f). To elucidate the calculation of the fluid frictional torque (T_f), a generalized formulation, denoted by Eq. (3b), is employed:

$$P_m + P_f = (T_m + T_f)\omega \quad (3b)$$

Here, P_m represents the power input corresponding to the mechanical torque (T_m), while P_f denotes the power input attributable to fluid frictional torque (T_f). Furthermore, ω stands for the angular speed of the impeller. By rearranging terms, the expression for the fluid frictional torque (T_f) is deduced, as per Eq. (3c):

$$T_f = \frac{(P_m+P_f)-(T_m\omega)}{\omega} \quad (3c)$$

This equation facilitates the computation of T_f by subtracting the product of T_m and ω from the sum of P_m and P_f, subsequently dividing by ω.

The first step to measure the fluid frictional torque by operating the pump without water at different speed and modify the results by subtracting the above value obtained at the first step.

2.2 Planning of Experiment

A factorial design with three factors was employed to investigate the impact of axial clearance, flow rate, and impeller speed on fluid frictional torque. Each factor was examined at three different levels. The values chosen are follows: axial clearance (0.6,1.2,1.8 mm), flow rate (8,10,12 L/min) and speed of impeller (800,1000,1200 rpm).

2.3 Response Surface Methodology

Response Surface Methodology (RSM) is a set of statistical and mathematical modeling techniques used to investigate the relationships between independent process parameters and their corresponding responses. The goal is to determined how these parameters affect the responses and then optimize them accordingly. Within the present investigation, the relationship linking fluid frictional torque with axial clearance, flow rate, and impeller speed is established as follows

$$T_f = \varphi_1(\omega, C_f, Q) \quad (1)$$

$$Y = \alpha_0 + \sum_{i=1}^{n} \beta_i X_i \sum_{i,j}^{n} \beta_i X_i X_j + \sum_{i=1}^{n} \beta_{ii} X_i^2 \quad (2)$$

Here, the term α_0 represents the constant term in the regression equation the coefficient $\beta_1, \beta_2 \ldots\ldots \beta_n$ along with $\beta_{11}, \beta_{22} \ldots\ldots \beta_{nn}$ signify the linear and quadratic terms respectively, additionally $\beta_{12}, \beta_{13} \ldots\ldots \beta_{n-1}$ denote the interacting terms within the model.

3. RESULTS AND DISCUSSIONS

3.1 Unifactorial Tests

Figure 2, 3 and 4 shows the outcomes of independent parameters on fluid frictional torque as functions of axial clearance (C_f), impeller speed (ω),and flow rate (Q). The results of fluid frictional torque denoted as T_f .

3.1.1 Effect of Impeller Speed on Fluid Frictional Torque

Figure 2 depict the relationship between impeller speed and frictional torque, while maintaining a constant axial clearance of 0.6 mm. The findings indicate that with an increase in impeller speed within the range of 800 to 1200 rpm, the fluid frictional torque demonstrate a corresponding rise of

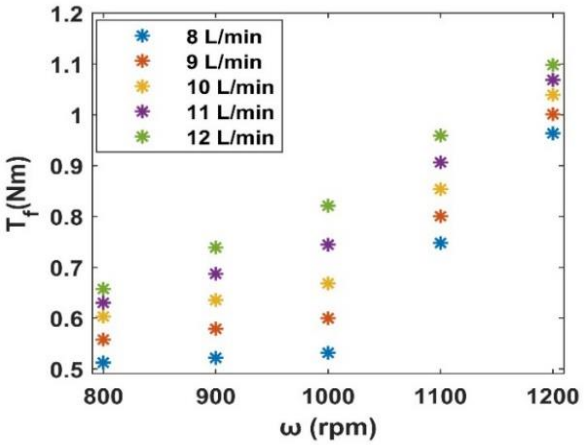

Fig. 2 Effect of ω and Q on fluid frictional torque(T_f) at constant axial clearance (C_f) of 0.6mm

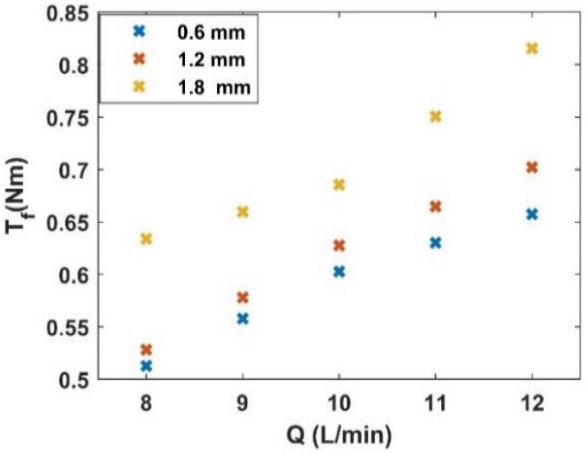

Fig. 3 Effect of Q and C_f on fluid frictional torque (T_f) at constant impeller speed (ω) of 800rpm

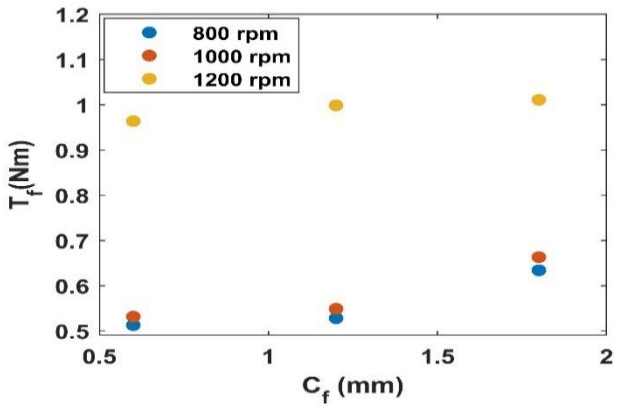

Fig. 4 Effect of C_f and ω on fluid frictional torque (T_f) at constant flow rate (Q) of 8L/min

64.79%, under a constant flow rate 8L/min condition. Additionally, the fluid frictional torque gradually increase as the flow rate escalates from 8 L/min to 12 L/min.

3.1.2 Effect of Flow Rate on Fluid Frictional Torque

Figure 3 illustrate the impact of flow rate on fluid frictional torque, maintaining a constant impeller speed of 800rpm. it's evident that an increase in flow rate corresponds to an increase in torque. The percentage change in fluid frictional torque with an axial clearance of 0.6mm, as the flow rate escalates from 8L/min to 12L/min is 21.53%. The plotted data demonstrates a gradual rise in fluid frictional torque from 0.6mm to 1.2mm axial clearance, with a notable spike in values observed when the axial clearance shifts from 1.2mm to 1.8mm.

3.1.3 Effect of Axial Clearance on Fluid Friction Torque.

The fluid frictional torque increase as we increase axial clearance. The fluid frictional torque increase by 19.04 %, at a constant speed of 800rpm. while changing the axial clearance from 0.6mm to 1.8mm. Hence, the unifactorial test suggest a strong correlation among the parameters, providing insights into the dynamics of fluid frictional torque.

3.2 Statistical Analysis

Table 2 presents the response values for the factors: axial clearance C_f , impeller speed ω, and volumetric flow rate Q. The goal is to assess how different combinations of these mixing parameters (C_f , ω, Q) impact the overall variance of the results obtained using a full factorial design. The values of fluid frictional torque were computed according to Eq. (3c). The fluid frictional torque was measured within the ranges of 0.512Nm to 1.158Nm. Analysis of Variance (ANOVA) is a common statistical method used extensively to assess the significance of independent variables on dependent variables. ANOVA does not directly analyse the data, but instead, it quantifies the percentage of contribution that each factor makes in explaining the variability (variance) observed in the data. Table 3 Shows the ANOVA results for fluid frictional torque. We can see that speed of impeller ω is the most influential factor. Its contribution is 68.21%. The next largest factor affecting frictional torque is volumetric flow rate Q followed by axial clearance. Their contributions are 16.13% and 3.01%. The interaction between three factors have contribution less than 1.5%. Hence, no significant contributions in calculating fluid frictional torque.

The regression models serve as valuable tools for forecasting the response parameters concerning the input control parameters. Figure 5 illustrate the difference between predicted and actual value of fluid frictional toque. The graph illustrates that the quadratic model effectively represents the system within the specified experimental domain. The comparative analysis confirms that the predicted values of the output parameter closely align with the experimentally recorded readings. To gain deeper insights into the interaction effects of variables on the response factor, Three-dimensional plots for measured responses and contour graphs were generated based on the model equations provided in Eq. (4). As this model incorporates three variables, one variable was maintained at the center level in each plot. Thus, a total of three response surface plots were generated to illustrate the response. Figure 6a-c shows the effect of impeller speed ω has more significance effect on fluid frictional torque as compared to the effect of axial clearance C_f and flow rate Q. Figure 6b illustrates that an increases in both C_f, Q Lead to increase fluid frictional torque. Although the impeller speed ω has highest contribution as shown in Table 3, the effect of both axial clearance C_f and flow rate Q also important factor for determine fluid frictional torque in centrifugal pump. To verify the validation, confirmation test was carried out for predicted and experimental values shown in Table 4. The calculated error, with the disparity between experimental and predicted values for T_f being less than 5%, underscores the high precision and reliability of the model's predictions.

$$T_f = 1.961 - 0.004 * \omega + 0.066 * Q - 0.030 * C_f - 0.000047 * \omega * Q - 0.000099 * \omega * C_f - 0.0053 * C_f * Q + 3.194 * 10^{-6} * \omega^2 + 0.001825 * Q^2 + 0.1063 * {C_f}^2 \quad (4)$$

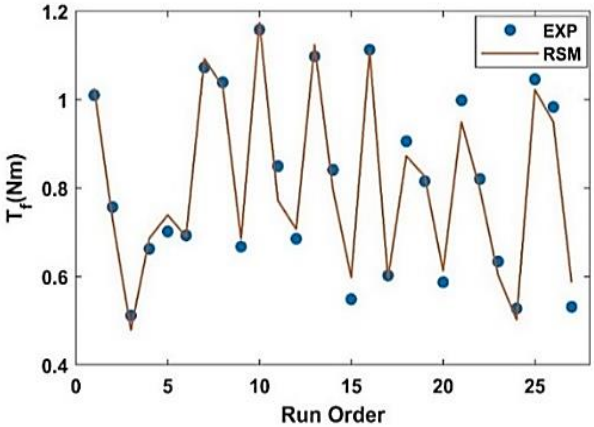

Fig. 5 Measured and predicted value of T_f

Table 2 Experimental results for fluid frictional torque

Std. order	Run order	ω (rpm)	Q (L/min)	C_f (mm)	T_f (Nm)
21	1	1200	8	1.8	1.0100
12	2	800	12	0.6	0.7572
9	3	800	8	0.6	0.5120
11	4	1000	8	1.8	0.6629
15	5	800	12	1.2	0.7021
22	6	1000	10	1.2	0.6934
25	7	1200	10	1.8	1.0730
5	8	1200	10	0.6	1.0390
23	9	1000	10	0.6	0.6679
27	10	1200	12	1.8	1.1580
6	11	1000	10	1.8	0.8498
17	12	800	10	1.8	0.6854
20	13	1200	12	0.6	1.0980
3	14	1000	12	1.2	0.8412
19	15	1000	8	1.2	0.5488
24	16	1200	12	1.2	1.1132
14	17	800	10	0.6	0.6027
13	18	1000	12	1.8	0.9057
26	19	800	12	1.8	0.8155
2	20	800	10	1.2	0.5874
1	21	1200	8	1.2	0.9985
18	22	1000	12	0.6	0.8207
16	23	800	8	1.8	0.6339
10	24	800	8	1.2	0.5280
8	25	1200	10	1.2	1.0460
7	26	1200	8	0.6	0.9835
4	27	1000	8	0.6	0.5314

Table 3 ANOVA results for fluid frictional torque

Sources	SM	DOF	MS	F-valve	P-valve	Cont. %	Remarks
Model	1.090	9	0.1207	74.69	< 0.0001		Significant
A-A	0.758	1	0.7585	469.35	< 0.0001	68.21	Significant
B-B	0.180	1	0.1805	111.7	< 0.0001	16.13	Significant
C-C	0.034	1	0.034	21.01	< 0.0001	3.01	Significant
AB	0.004	1	0.0042	2.58	0.3011	0.003	
AC	0.001	1	0.0017	1.05	0.0511	0.0015	
BC	0.000	1	0.0005	0.3026	0.9764	0.0004	
A^2	0.097	1	0.0979	60.61	< 0.0001	0.0881	
B^2	0.000	1	0.0003	0.1979	0.9139	0.0002	
C^2	0.008	1	0.0088	5.45	0.0803	0.0079	
Residual	0.027	17	0.0016				
Total	1.11	26					

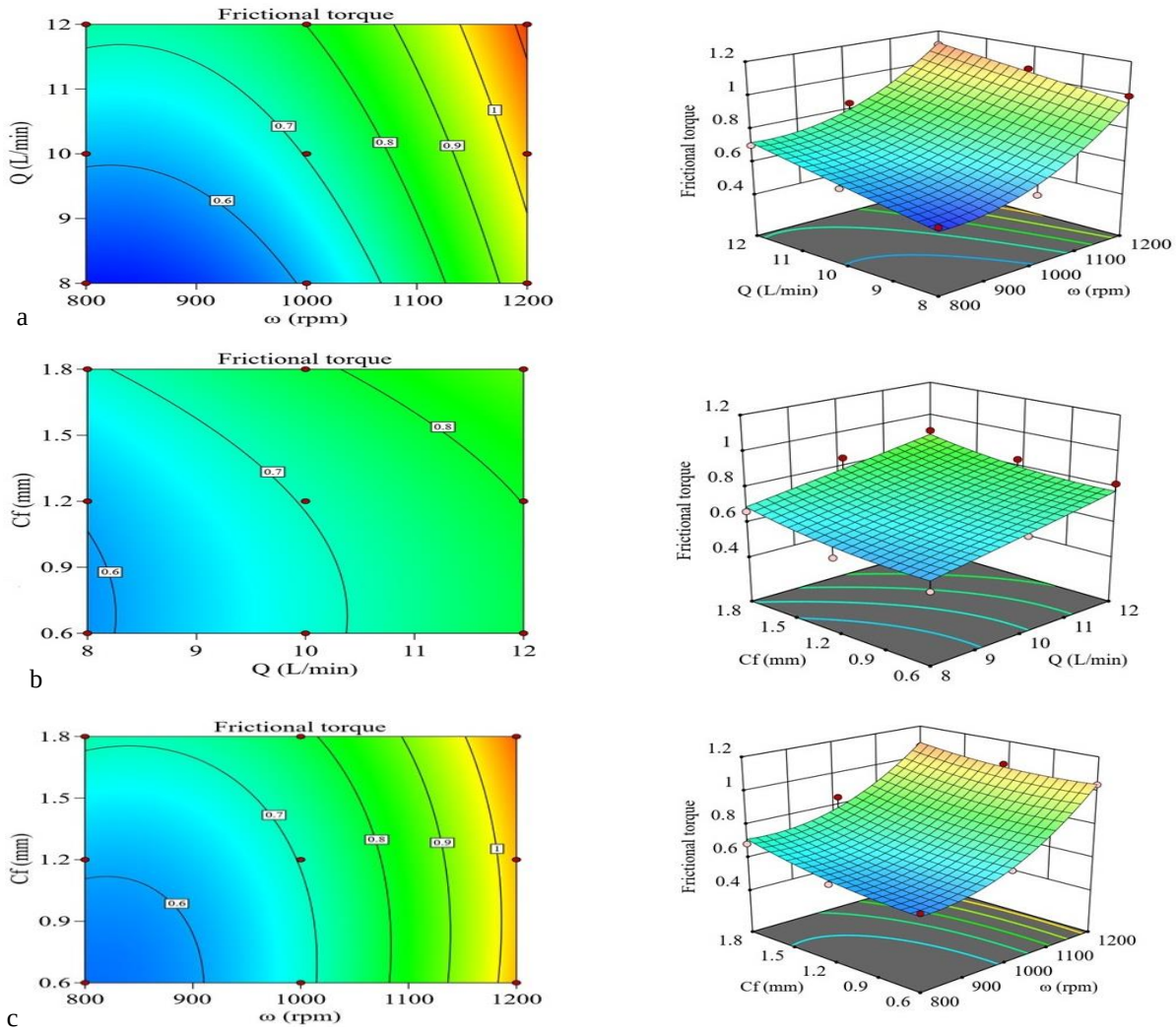

Fig. 6 Contours graphs for fluid frictional torque (T_f) depending on, ω, C_f ,and Q

Table 4 Confirmation test on experimental and predictive result

Test	ω (rpm)	C_f (mm)	Q (L/min)	Exp. value	Pre. value	Error
T_f (Nm)	850	0.6	8.5	0.525	0.5091	3.02%

3.4 Modeling by Artificial Neural Network (ANN)

Recent studies have focused on Artificial neural networks (ANNs) based model due to their ability to model highly non leaner processes. These models use computational techniques that mimic the human brain to perform a variety of tasks, such as logical reasoning, thinking, and studying. This has to be done by interconnecting neurons through massive parallel computing of data and information. Figure 7 shows the architecture of ANN model, having three layers, an input layer, one hidden layer and an output layer.

The symbol of circles representing the neurons and the lines shows the flow of information to the neurons. The learning method of ANN is back propagation algorithm. The neurons in one layer connected to other neurons in

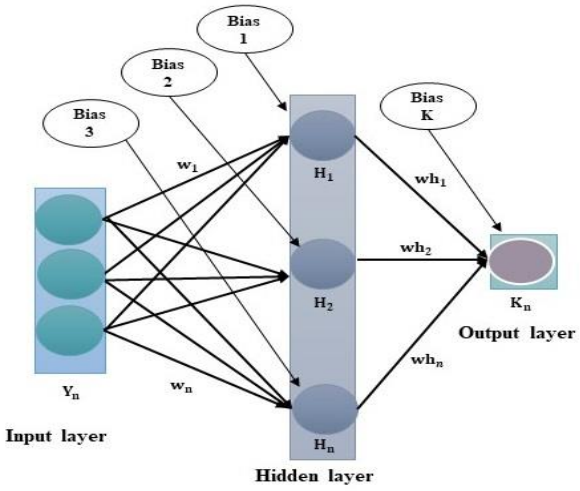

Fig.7 Architecture of ANN model

another layer with weighted connection. The signals are transferred from one neuron to other neurons via an activation function. The ANN model is called trained when weights and biases are stable Acherjee et al. (2011). The flow diagram of ANN phases is depicted in Fig. 8, including the steps of initializing and obtaining the suitable architecture for investigation. The artificial neural network widely used as a deep learning tool for its ability to handle non linearity, generalization, adaptability and large datasets.

3.5 Modeling of Fluid Frictional Torque Using ANN

The fluid frictional torque is modelled using single layer feed forward with the help of back propagation algorithm. In this research, an input layer with three neurons, one hidden layer with three neurons and an output layer with one neuron employed. The effectiveness of the ANN model depends on number of neurons present in hidden layer. As a result, variation of neurons in hidden layer tested to get an effective architecture as shown in Table 5. The performance metrics of optimum ANN architecture, suggested by majority researcher is RMSE (root mean square error) defined as follow:

$$RMSE = \sqrt{\frac{1}{N}\sum_{i=1}^{N}(Yo_i - Yp_i)^2} \quad (5)$$

Where, Yo_i and Yp_i are observed and predicted values, respectively, and N is number of experiments.

Table 5 Comparing RMSE for different architectures for fluid friction torque

S.I No	Architectures	RMSE
1	3-2-1	0.0737
2	**3-3-1**	**0.0341**
3	3-4-1	0.0428

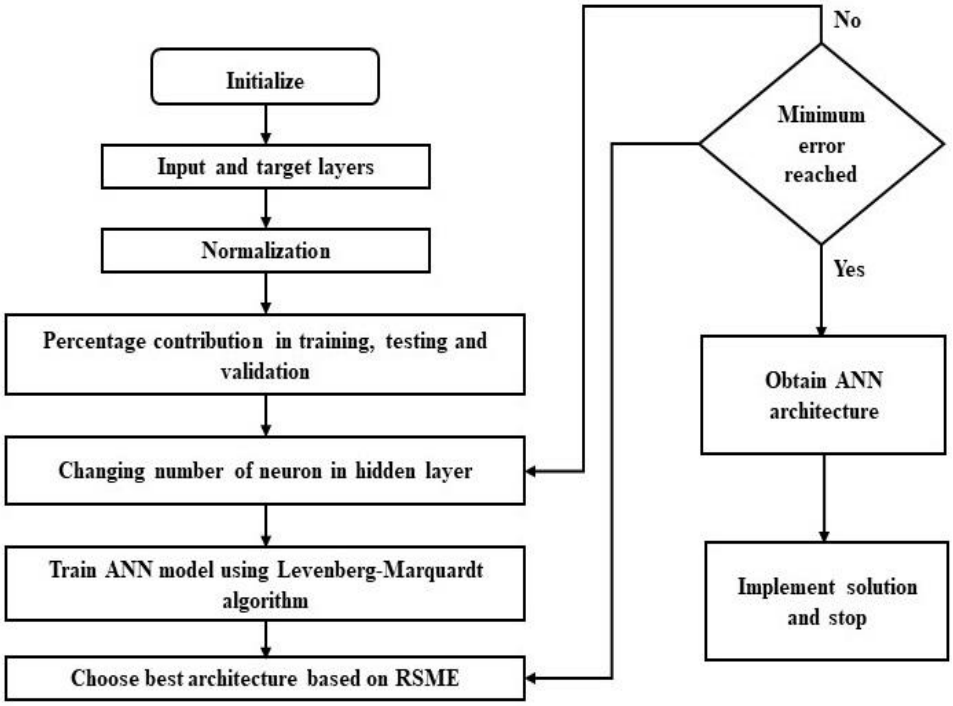

Fig. 8 Flow diagram of ANN model

3.5.1 Definition of Input and Output Layers

The nodes and the input parameters are equal in number in input layer. The experimental data of fluid frictional torque is transmitted through the input layer to hidden layer with the help of activation function and weighted connections. Eventually, the information from the hidden layer send to output layer. Where, the error between expected and desired output (targets) assesses. The output layer has same number of nodes corresponding to output parameters. Three parameters (Axial clearance, impeller speed and flow rate) considered in input, where fluid frictional torque considered output in a single layer artificial neural networks to create the model.

3.5.2 Definition of Hidden Layer

As the input and output layer has same number of neurons corresponding to their process parameters, the number of neurons in hidden layer changed to obtain best ANN architecture. Excess of neurons in hidden layer cause over fitting problems, where a smaller number of neurons in hidden layer led to under fitting problems. So, a rigors investigation should give to determined number of neurons in hidden layer as it impact on overall performance of ANN architecture. The heuristic method is used to determine the minimum and maximum numbers of neurons within a range in hidden layer. The Majesty's department of trade and industry (MTI) defined the lower limit of neurons in hidden layer (Garcia-Romeu et al., 2010).

$$N_{min} = \frac{NI+NO}{2} \quad (6)$$

After obtaining minimum number of neurons for hidden layer, continuously adding one more neuron in hidden layer to check the efficacy of the ANN architecture. In hidden layer, the maximum number of neurons is defined by Lippmann (1988).

$$N_{max} = NO * (NI + 1) \quad (7)$$

Where, N_{min} and N_{max} represents the minimum and maximum neurons in hidden layer and NI, NO denote number of neurons in input and output layer.

3.6 Training of The ANN Model

The artificial neural network model is train using experimental data, employing feed forward and back propagation algorithm. The artificial neural network architecture of fluid frictional torque is shown in Fig. 9. the training phases of ANN model such as training, validation and testing is done using MATLAB 2022 platform.

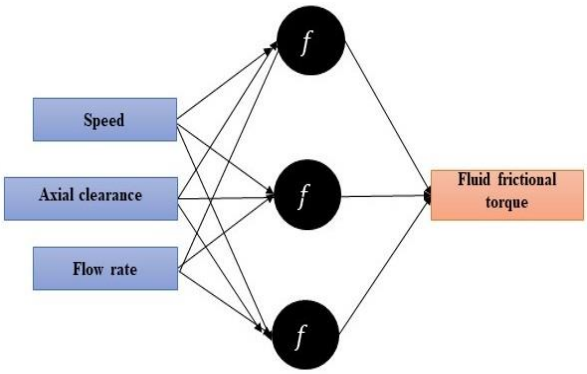

Fig. 9 ANN architecture for fluid frictional torque

The experimental data segregated into three sets for training, validation and testing. The percentage contributions of experimental sets are shown in Table 6.

Table 6 Training Phases of Experimental Sets

Training phases	Per. cont. (%)	Experimental sets
Training	75	19
Validation	15	4
Testing	15	4

This segregated data enables the network to learn, while using separate validation and testing sets to evaluate its performance and assess its generalization capabilities. The ANN model has different layers in its architecture including input, output and hidden layer. Input layer does not have any transfer function whereas output and hidden layer have a tansignoid transfer function. These transfer function allow to produce output, which is necessary for performance prediction of ANN model. Figure 10 displays the convergence of the artificial neural network (ANN) architecture post-training. It presents the evolution of the ANN model across training epochs. The highest validation performance of 3-3-1 ANN architecture at epoch 9 is 0.0020481, suggesting that the model performance is optimal based on validation set evaluation at this training phase. By employing the Levenberg-Marquardt Learning Algorithm in conjunction with a precise ANN architecture and training approach, accurate forecasting of fluid frictional torque is achievable. The regression plots depicted in Fig. 11 are utilized for assessing the adequacy of the ANN model's predictions. In Fig. 11a, there is a comparison between the forecasted and observed data for the training patterns. From this figure, it's clear that the forecasted values exhibit minimal error, showcasing a noteworthy degree of accuracy within the training dataset. In Fig. 11b, the observed and forecasted data for the validation patterns are compared, while in Fig. 11c, the comparison is made for the testing patterns. These plots exhibit a near match between the forecasted and observed response values. The close alignment of data points in both the validation and testing plots underscores the model's exceptional capacity to generalize and produce accurate predictions. The effectiveness of the developed ANN model is further evaluated by R^2 value of 0.99, depicted in Fig. 11d. These observations confirm the efficacy of the artificial neural network (ANN) model, reinforcing confidence in its capacity to provide accurate fluid frictional torque prediction.

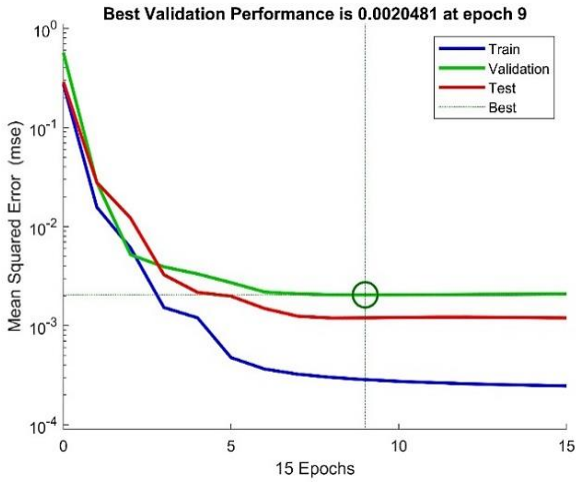

Fig. 10 Conversion diagram of 3-3-1 ANN architecture

3.5 Comparison Between RSM and ANN Models

The coefficient of determination (R^2), measures the proportion of the variance in the dependent variable that is predictable from the independent variables. These values indicate the goodness of fit of the models. A higher (R^2), value suggests that a larger proportion of the variance in the dependent variable is explained by the independent variables, indicating a better fit of the model to the data. The ANN model has a slightly higher (R^2), value (99.19%) compared to the RSM model (97.96%). This suggests that the ANN model explains a slightly larger proportion of the variance in the fluid frictional torque compared to the RSM model However, both models

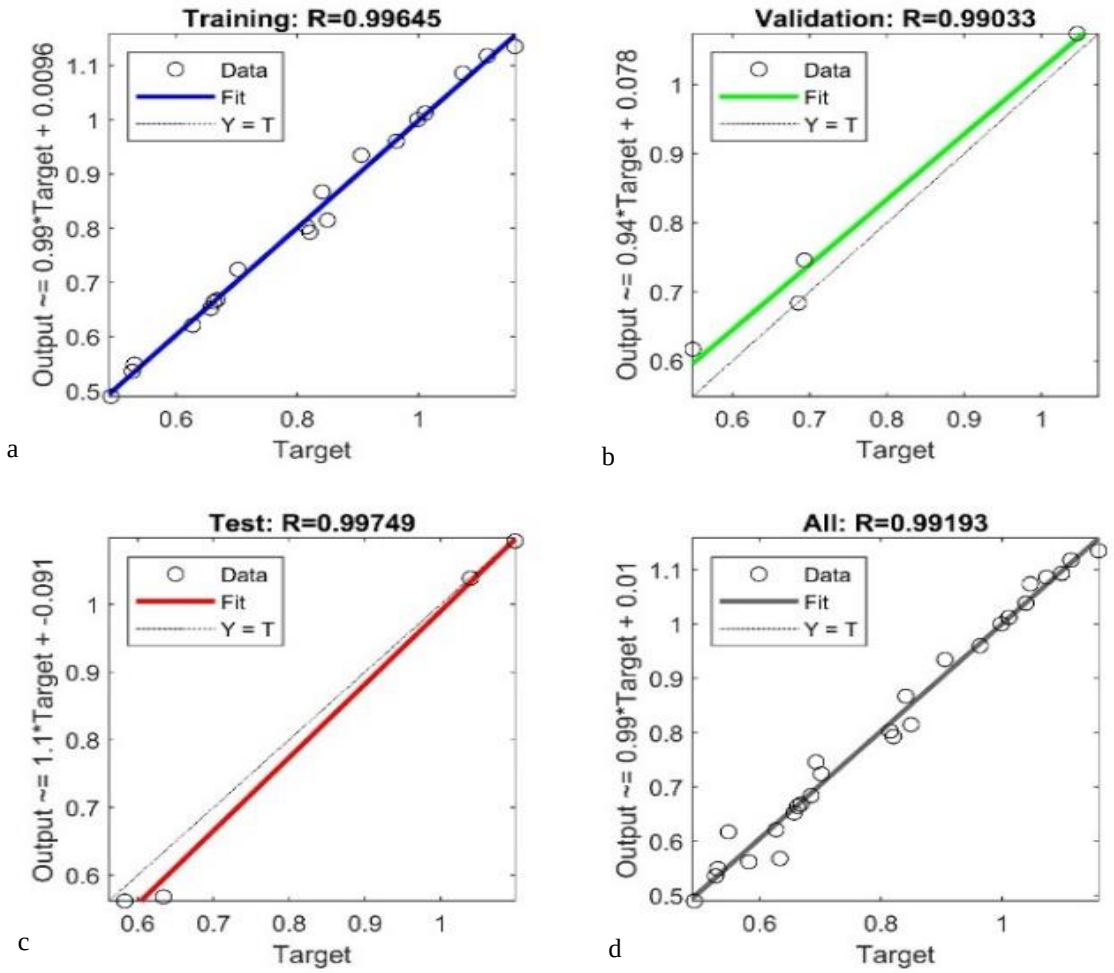

Fig. 11 Regression plots comparing the actual and predicted data for fluid frictional torque

Table 7 Goal and ranges for optimization of fluid frictional torque

Name	Goal	Lower limit	Upper limit	Lower weight	Upper weight	Importance
ω (rpm)	In range	800	1200	1	1	3
C_f (mm)	In range	0.6	1.8	1	1	3
Q (L/min)	In range	8	12	1	1	3
T_f (Nm)	Minimize	0.512	1.158	1	1	3

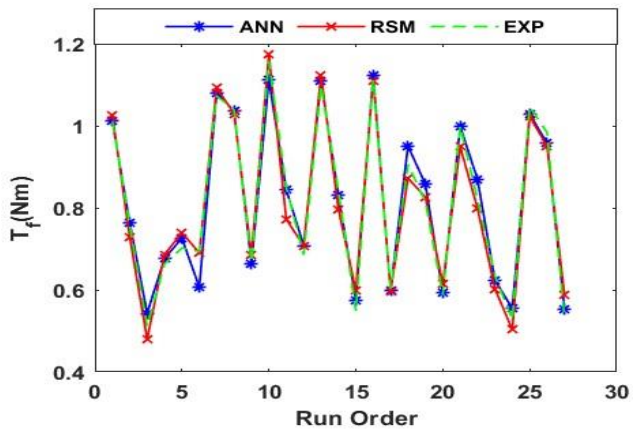

Fig. 12 Comparison between experimental value of torque and the predicted values by RSM and ANN

have high (R^2), values, indicating that they both provide good fits to the data and can effectively predict the fluid frictional torque based on the input variables. To illustrate the comparison between RSM and ANN models, Fig.12 depict the observed and forecasted values of fluid frictional torque.

4. OPTIMIZATION OF RESPONSE USING DESIRABILITY FUNCTIONS

The desirability function is a tool used in multi-response optimization to quantify how desirable or favorable certain values of response variables are within a given range. It assigns a numerical score, typically ranging from 0 to 1, to each response variable value based on its desirability. Within these defined ranges, assign desirability scores to each value. A score of 1 indicates that

the value is perfectly desirable, while a score of 0 indicates that it is entirely undesirable. This can be done using various aggregation methods, such as the geometric mean or weighted sum (Chabbi et al.2017).

$$D = (d_1 * d_2 * \dots \dots * d_n)^{1/n} = (\prod_{i=1}^{n} d_i)^{1/n} \quad (8)$$

$$F(x) = -D \quad (9)$$

In the context of simultaneous optimization, we assign a desirability d_i to each i^{th} targeted output, along with a corresponding weighting w_i and the total number of responses n. Each response is then associated with both a low and high value for every goal. When the objective is to minimize, the desirability takes the following form:

$$\begin{cases} d_i = 1 \text{ response } < \text{low value} \\ 0 \le d_i \ll 1 \text{ low to high} \\ d_i = 1 \text{ response } > \text{high value} \end{cases} \quad (10)$$

For optimizing responses using the desirability function, Design of Expert software is utilized. The factor ranges for combined optimization are detailed in Table 7. In the case of optimization, a notable advantage is the achievement of minimum fluid frictional torque, aligning with industry objectives. Fig.13 presents the contour graph illustrating the optimal value of the rotational speed of impeller ω, flow rate Q and axial clearance C_f with desirability of 1. The optimal values are as follows: $\omega = 888.94$, $Q = 8.026$ and $C_f = 0.619$ .The optimum fluid frictional torque is 0.499Nm

5. CONCLUSIONS

This study examines the impact of axial clearance, flow rate, and impeller speed on fluid frictional torque. Furthermore, it seeks to optimize fluid frictional torque to identify the optimal parameters for a centrifugal pump, aiming to minimize fluid frictional torque. Based on the

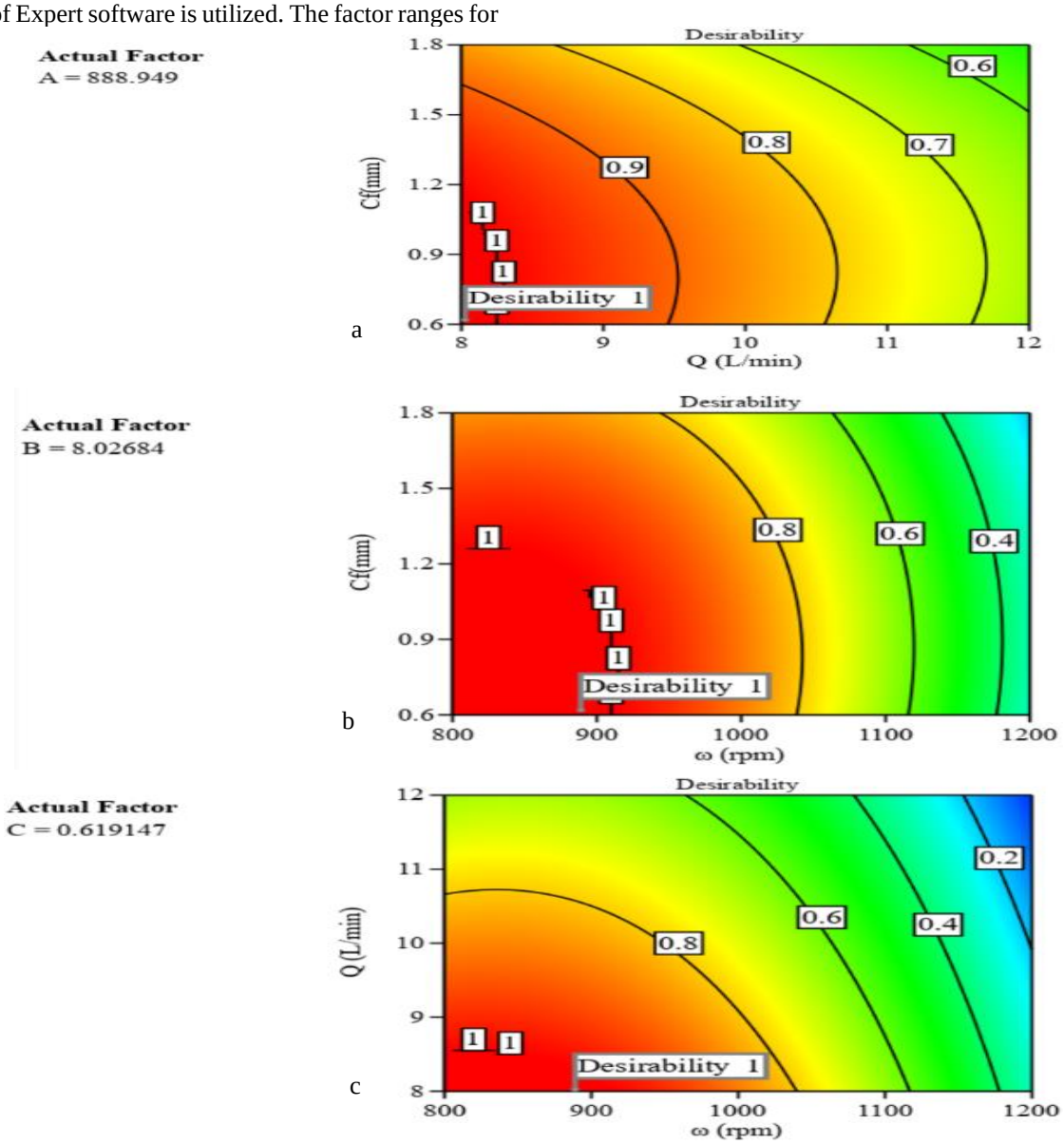

Fig. 13 Contour graph for desirability: (a) ω = 888.94, (b) Q =8.026 and(c) C_f =0.619

previously discussed results, the following conclusions have been drawn.

1. In unifactorial test, the fluid frictional torque increasing as we increase the impeller speed, axial clearance and flow rate. For calculating fluid frictional torque all parameters are significant. However, ω is the most significant parameter in calculating fluid frictional torque followed by Q and C_f . The percentage change in fluid frictional torque, while changing the parameters(ω, Q, C_f) is 46.86%. 31.11%,19.04 % respectively.
2. The results of ANOVA analysis for fluid frictional torque proved that the speed of impeller is the most important affecting parameter followed by volumetric rate and axial clearance. The contribution of ω, Q, C_f on T_f are 68.21%,16.13%,3.01% respectively.
3. The correlation coefficients of the predictive models by RSM and ANN for fluid frictional torque found to be 97.96%,99.19% respectively. Hence, the developed models are deemed reliable and hold significant industrial relevance, as they enable accurate predictions within the range of actual experimental data.
4. The confirmation test results indicate that the developed models are effective in predicting the responses. The error in measuring for fluid frictional torque is less than 5%.
5. The ANN model demonstrates greater robustness and reliability compared to the RSM model, as evidenced by its higher values of correlation coefficients (R^2).
6. The optimal parameters for minimum fluid frictional torque are following $\mathrm{Q} = 8.026\ \mathrm{L/min}$, $C_f = 0.619mm$ and $\omega = 888.90\ rpm$.

ACKNOLEDGEMENTS

I am grateful to the Mechanical Engineering Department for generously providing laboratory access. Special thanks to all the authors for their invaluable contributions to this research**.**

CONFLICT OF INTEREST

The authors assert no competing interests in this research

AUTHORS CONTRIBUTIONS

Kamal Singh contributed to study design, data analysis and interpretation, and writing the original draft, while **Achhaibar Singh** and **Dinesh Kumar Singh** provided supervision, critical feedback, and review

REFRENCES

Acherjee, B., Mondal, S., Tudu, B., & Misra, D. (2011). Application of artificial neural network for predicting weld quality in laser transmission welding of thermoplastics. *Applied Soft Computing*, *11*(2), 2548-2555. http://dx.doi.org/10.1016/j.asoc.2010.10.005

Alzubi, J., Nayyar, A., & Kumar, A. (2018, November). *Machine learning from theory to algorithms: an overview*. Journal of Physics: Conference Series (Vol. 1142, p. 012012). IOP Publishing. https://doi.org/10.1088/1742-6596/1142/1/012012

Chabbi, A., Yallese, M. A., Nouioua, M., Meddour, I., Mabrouki, T., & Girardin, F. (2017). Modeling and optimization of turning process parameters during the cutting of polymer (POM C) based on RSM, ANN, and DF methods. *The International Journal of Advanced Manufacturing Technology*, *91*, 2267-2290. https://doi.org/ 10.1007/s00170-016-9858-8

Derakhshan, S., Mohammadi, B., & Nourbakhsh, A. (2008). Incomplete sensitivities for 3D radial turbomachinery blade optimization. *Computers & Fluids*, *37*(10), 1354-1363. https://doi.org/10.1016/j.compfluid.2008.01.002

Ekradi, K., & Madadi, A. (2020). Performance improvement of a transonic centrifugal compressor impeller with splitter blade by three-dimensional optimization. *Energy*, *201*, 117582. https://doi.org/10.1016/j.energy.2020.117582

Gan, X., Pei, J., Wang, W., Yuan, S., & Lin, B. (2023). Application of a modified MOPSO algorithm and multi-layer artificial neural network in centrifugal pump optimization. *Engineering Optimization*, *55*(4), 580-598. https://doi.org/10.1080/0305215X.2021.2015585

Gao, Z., Zhu, W., Lu, L., Deng, J., Zhang, J., & Wuang, F. (2014). Numerical and experimental study of unsteady flow in a large centrifugal pump with stay vanes. *Journal of Fluids Engineering*, *136*(7), 071101. https://doi.org/10.1115/1.4026477

Garcia-Romeu, M. L., Ceretti, E., Fiorentino, A., & Giardini, C. (2010, January). *Forming force prediction in two-point incremental forming using Backpropagation neural networks in combination with Genetic Algorithms.* International Manufacturing Science and Engineering Conference (Vol. 49477, pp. 99-106). http://dx.doi.org/10.1115/MSEC2010-34142

Ghadimi, B., Nejat, A., Nourbakhsh, S. A., & Naderi, N. (2019). Multi-objective genetic algorithm assisted by an artificial neural network metamodel for shape optimization of a centrifugal blood pump. *Artificial Organs*, *43*(5), E76-E93. https://doi.org/10.1111/aor.13366

González, J., & Santolaria, C. (2006). Unsteady flow structure and global variables in a centrifugal pump. *ASME. Journal of Fluids Engineering*, *128*(5): 937–946. https://doi.org/10.1115/1.2234782

Gülich, J. F. (2003). Disk friction losses of closed turbomachine impellers. *Forschung im Ingenieurwesen*, *68*(2), 87-95. https://doi.org/10.1007/s10010-003-0111-x

Han, X., Kang, Y., Sheng, J., Hu, Y., & Zhao, W. (2020). Centrifugal pump impeller and volute shape optimization via combined NUMECA, genetic algorithm, and back propagation neural network. *Structural and Multidisciplinary Optimization*, *61*, 381-409. https://link.springer.com/article/10.1007/s00158-019-02367-8

Kaupert, K. A., & Staubli, T. (1999). The unsteady pressure field in a high specific speed centrifugal pump impeller—part I: influence of the volute. *ASME. Journal of Fluids Engineering*, *121*(3), 621–626. https://doi.org/10.1115/1.2823514

Kergourlay, G., Younsi, M., Bakir, F., & Rey, R. (2007). Influence of splitter blades on the flow field of a centrifugal pump: test-analysis comparison. *International Journal of Rotating Machinery*, 2007(1) https://doi.org/10.1155/2007/85024

Lippmann, R. P. (1988). An introduction to computing with neural nets. *Acm Sigarch Computer Architecture News*, *16*(1), 7-25. https://doi.org/10.1145/44571.44572

Liu, H., Wang, K., Yuan, S., Tan, M., Wang, Y., & Dong, L. (2013). Multicondition optimization and experimental measurements of a double-blade centrifugal pump impeller. *Journal of Fluids Engineering*, *135*(1), 011103. https://doi.org/10.1115/1.4023077

Ma, S. B., Afzal, A., & Kim, K. Y. (2018). Optimization of ring cavity in a centrifugal compressor based on comparative analysis of optimization algorithms. *Applied Thermal Engineering*, *138*, *633-647*.. https://doi.org/10.1016/j.applthermaleng.2018.04.04

Massoudi, S., Picard, C., & Schiffmann, J. (2022). Robust design using Mult objective optimisation and artificial neural networks with application to a heat pump radial compressor. *Design Science*, *8*, e1. https://doi.org/10.1017/dsj.2021.25

Owoyele, O., & Pal, P. (2021a). A novel active optimization approach for rapid and efficient design space exploration using ensemble machine learning. *Journal of Energy Resources Technology*, *143*(3), 032307. https://doi.org/10.1115/1.4049178

Owoyele, O., & Pal, P. (2021b). A novel machine learning-based optimization algorithm (ActivO) for accelerating simulation-driven engine design. *Applied Energy*, *285*, 116455. https://doi.org/10.1016/j.apenergy.2021.116455

Pedersen, N., Larsen, P. S., & Jacobsen, C. B. (2003). Flow in a centrifugal pump impeller at design and off-design conditions—part I: particle image velocimetry (PIV) and laser Doppler velocimetry (LDV) measurements. *ASME. Journal of Fluids Engineering*, *125(1): 61–72*. https://doi.org/10.1115/1.1524585

Pei, J., Gan, X., Wang, W., Yuan, S., & Tang, Y. (2019). Multi-objective shape optimization on the inlet pipe of a vertical inline pump. *Journal of Fluids Engineering*, *141*(6), 061108. https://doi.org/10.1115/1.4043056

Pei, J., Yuan, S., Benra, F. K., & Dohmen, H. J. (2012). Numerical prediction of unsteady pressure field within the whole flow passage of a radial single-blade pump. ASME, Journal of Fluids Engineering , 134(10). https://doi.org/10.1115/1.4007382

Qiu, J. T., Yang, C. J., Dong, X. Q., Wang, Z. L., Li, W., & Noblesse, F. (2018). Numerical simulation and uncertainty analysis of an axial-flow waterjet pump. *Journal of Marine Science and Engineering*, *6*(2), 71. https://doi.org/10.3390/jmse6020071

Song, X., Li, Y., Huang, R., & Luo, X. (2024, February). *Impeller optimization using a machine learning-based algorithm with dynamic sampling method and flow analysis for an axial flow pump*. Journal of Physics: Conference Series (Vol. 2707, No. 1, p. 012154). IOP Publishing. https://10.1088/1742-6596/2707/1/012154

Song, X., Yu, W., Pan, X., & Luo, X. (2021, May). *Energy balance analysis for a canned motor pump used for heat supply system.* Journal of Physics: Conference Series (Vol. 1909, No. 1, p. 012072). IOP Publishing. https://doi.org/10.1088/1742-6596/1909/1/012072

Stel, H. A. G. N. C., Amaral, G. D. L., Negrao, C. O. R., Chiva, S., Estevam, V., & Morales, R. E. M. (2013). Numerical analysis of the fluid flow in the first stage of a two-stage centrifugal pump with a vaned diffuser. *Journal of Fluids Engineering*, *135*(7), 071104. https://doi.org/10.1115/1.4023956

Wang, G. G., & Shan, S. (2006, January). *Review of metamodeling techniques in support of engineering design optimization.* International Design Engineering Technical Conferences and Computers and Information in Engineering Conference (Vol. 4255, pp. 415-426). https://doi.org/10.1115/DETC2006-99412

Wang, W., Osman, M. K., Pei, J., Gan, X., & Yin, T. (2019). Artificial neural networks approach for a multi-objective cavitation optimization design in a double-suction centrifugal pump. *Processes*, *7*(5), 246. https://doi.org/10.3390/pr7050246

Xiang, H., Chen, J., Cheng, J., & Song, X. (2022). Blade number selection for a splittered mixed-flow compressor impeller using improved loss model. *International Journal of Turbo & Jet-Engines*, *39*(4), 549-564. https://doi.org/10.1515/tjj-2020-0008

Xie, R. S., Tang, F. P., Yang, F., & Xiang, C. (2018, July). *Effect of the flow in blade root-leakage on hydraulic characteristic in axial flow pump system.* IOP Conference Series: Earth and Environmental Science (Vol. 163, No. 1, p. 012123). IOP Publishing. https://doi.org/10.1088/1755-1315/163/1/012123

Yang, F., Li, Z., Fu, J., Lv, Y., Ji, Q., & Jian, H. (2022a). Numerical and experimental analysis of transient

flow field and pressure pulsations of an axial-flow pump considering the pump–pipeline interaction. *Journal of Marine Science and Engineering*, *10*(2), 258. https://doi.org/10.3390/jmse10020258

Yang, F., Lin, Z., Li, J., Nasr, A., Cong, W., & Li, C. (2022b). Analysis of internal flow characteristics and structure optimization of vertical submersible axial flow pump device. *Advances in Mechanical Engineering*, *14*(5), 16878132221100641. https://doi.org/10.1177/16878132221100641

Yuan, Y., & Yuan, S. (2017). Analyzing the effects of splitter blade on the performance characteristics for a high-speed centrifugal pump. *Advances in Mechanical Engineering*, *9*(12), 1687814017745251. https://doi.org/10.1177/1687814017745251

Zhang, D., Shi, W., Van Esch, B. B., Shi, L., & Dubuisson, M. (2015). Numerical and experimental investigation of tip leakage vortex trajectory and dynamics in an axial flow pump. *Computers & Fluids*, *112*, 61-71. https://doi.org/10.1016/j.compfluid.2015.01.010

Zhang, W., Tang, F., Shi, L., Hu, Q., & Zhou, Y. (2020). Effects of an inlet vortex on the performance of an axial-flow pump. *Energies*, *13*(11), 2854. https://doi.org/10.3390/en13112854

Zhao, B., Wang, Y., Chen, H., Qiu, J., & Hou, D. (2015). Hydraulic optimization of a double-channel pump's impeller based on multi-objective genetic algorithm. *Chinese Journal of Mechanical Engineering*, *28*(3), 634-640. https://doi.org/10.3901/CJME.2015.0116.016

Zhao, X., Chen, T., Huang, B., & Wang, G. (2022, April). *Numerical analysis of the cavitating flow in an axial flow waterjet pump with special emphasis on the tip leakage flow and tip leakage vortex.* Journal of Physics: Conference Series (Vol. 2217, No. 1, p. 012018). IOP Publishing. https://doi.org/10.1088/1742-6596/2217/1/012018

Zhao, X., Liu, T., Huang, B., & Wang, G. (2020). Combined experimental and numerical analysis of cavitating flow characteristics in an axial flow waterjet pump. *Ocean Engineering*, *209*, 107450. https://doi.org/10.1016/j.oceaneng.2020.107450

Zhu, H., Bo, G., Zhou, Y., Zhang, R., & Cheng, J. (2018). Pump selection and performance prediction for the technical innovation of an axial-flow pump station. *Mathematical Problems in Engineering*, *2018*. https://doi.org/10.1155/2018/6543109